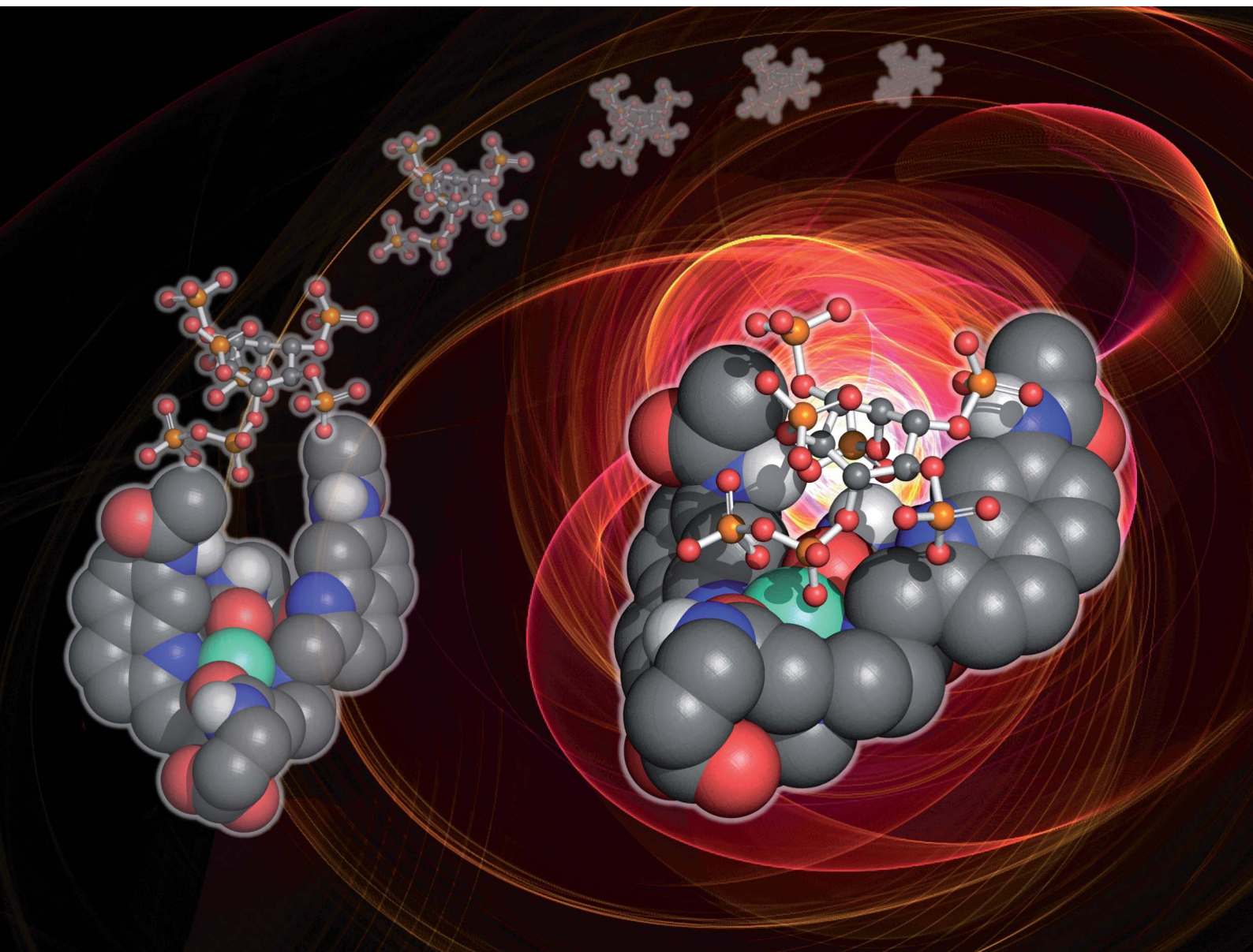


Chemical Science

Volume 14
Number 19
21 May 2023
Pages 4947–5228

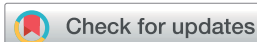
rsc.li/chemical-science



ISSN 2041-6539

EDGE ARTICLE

Barry V. L. Potter, Stephen J. Butler *et al.*
Expedient synthesis and luminescence sensing of the
inositol pyrophosphate cellular messenger 5-PP-InsP₅

Cite this: *Chem. Sci.*, 2023, 14, 4979

All publication charges for this article have been paid for by the Royal Society of Chemistry

Expedient synthesis and luminescence sensing of the inositol pyrophosphate cellular messenger 5-PP-InsP₅†

Megan L. Shipton,^{‡b} Fathima A. Jamion,^{‡a} Simon Wheeler,^{‡a} Andrew M. Riley,^{‡b} Felix Plasser,^{‡a} Barry V. L. Potter^{‡*b} and Stephen J. Butler^{‡*a}

Inositol pyrophosphates are important biomolecules associated with apoptosis, cell growth and kinase regulation, yet their exact biological roles are still emerging and probes do not exist for their selective detection. We report the first molecular probe for the selective and sensitive detection of the most abundant cellular inositol pyrophosphate 5-PP-InsP₅, as well as an efficient new synthesis. The probe is based on a macrocyclic Eu(III) complex bearing two quinoline arms providing a free coordination site at the Eu(III) metal centre. Bidentate binding of the pyrophosphate group of 5-PP-InsP₅ to the Eu(III) ion is proposed, supported by DFT calculations, giving rise to a selective enhancement in Eu(III) emission intensity and lifetime. We demonstrate the use of time-resolved luminescence as a bioassay tool for monitoring enzymatic processes in which 5-PP-InsP₅ is consumed. Our probe offers a potential screening methodology to identify drug-like compounds that modulate the activity of enzymes of inositol pyrophosphate metabolism.

Received 12th December 2022

Accepted 7th April 2023

DOI: 10.1039/d2sc06812e

rsc.li/chemical-science

Introduction

Inositol phosphates are highly phosphorylated small molecules of paramount importance to cellular signalling. *Myo*-inositol hexakisphosphate (InsP₆, also called phytate) is a ubiquitous molecule in eukaryotic cells that has critical roles in signal transduction and cellular regulation. Inositol pyrophosphates (PP-InsPs), derived from inositol phosphates such as InsP₆, possess one or more highly energetic phosphoanhydride bonds and represent the most highly phosphorylated species in nature. Because PP-InsPs are sensors and regulators of energy homeostasis in the cell they participate in a range of processes such as apoptosis, protein pyrophosphorylation, cell migration and cancer metastasis, intracellular trafficking, cell growth and kinase regulation^{1,2} with implications in disease.³

There are two groups of kinase enzymes in humans [InsP₆ kinases (IP6Ks) and PP-InsP₅ kinases (PPIP5Ks)] that can form pyrophosphate groups at either the 5-position or the 1-position of the phosphorylated inositol ring of InsP₆.⁴ These pyrophosphate groups can be cleaved through the action of a group of

promiscuous phosphatases called diphosphoinositol polyphosphate phosphohydrolases (DIPPs) (Fig. 1). The reversible interconversion between PP-InsP₅/InsP₆ may be considered as an ADP/ATP equivalent in protein dephosphorylation and bioenergetics,¹ hence the development of synthetic probes that can discriminate between pyrophosphorylated inositol polyphosphates and InsP₆ is of particular current interest.

The most abundant inositol pyrophosphate in mammals is 5-diphosphoinositol pentakisphosphate, 5-PP-InsP₅ (Fig. 1 and Scheme 1) whose intracellular concentration ranges between 0.5–5.0 μM.^{1,2} Determining the exact biological functions of 5-PP-InsP₅ and other such pyrophosphates is an ongoing pursuit

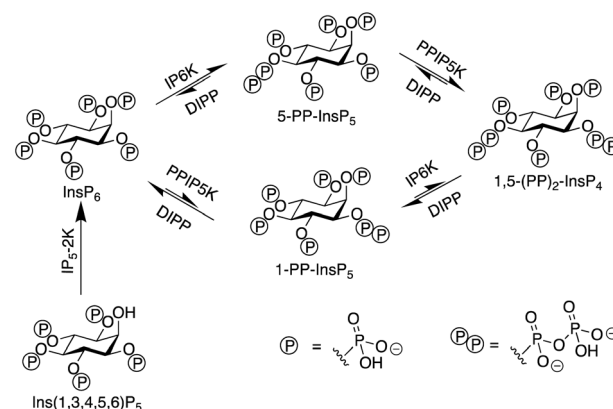


Fig. 1 The interconversion of inositol pyrophosphates in mammals.

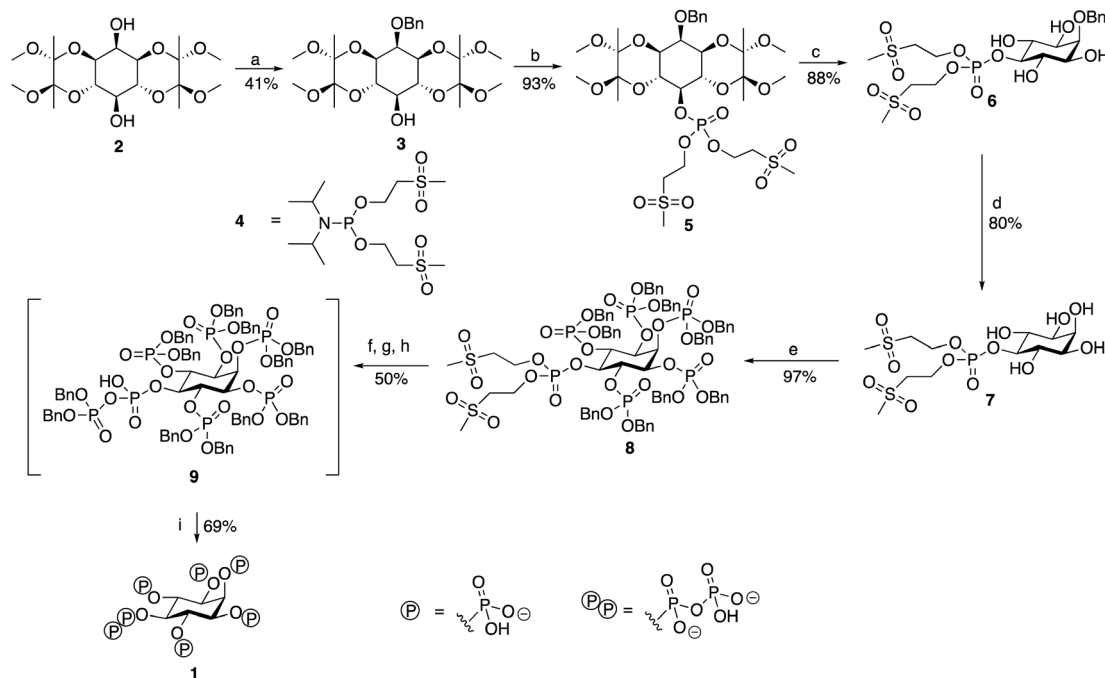
^aDepartment of Chemistry, Loughborough University, Epinal Way, Loughborough, LE11 3TU, UK. E-mail: S.J.Butler@lboro.ac.uk

^bMedicinal Chemistry & Drug Discovery, Department of Pharmacology, University of Oxford, Mansfield Road, Oxford OX1 3QT, UK. E-mail: barry.potter@pharm.ox.ac.uk

† Electronic supplementary information (ESI) available: Synthetic details, photophysical analysis of host-guest interactions. See DOI: <https://doi.org/10.1039/d2sc06812e>

‡ Equal contribution from both authors.





Scheme 1 Synthesis of 5-PP-InsP₅. Reagents and conditions: (a) DMF, NaH, BnBr; (b) (1) DCM, 5-phenyl-1*H*-tetrazole, (OMSE)₂PN(*i*Pr)₂ reagent 4, 16 h (2) *m*CPBA, −78 °C-RT; (c) TFA, H₂O; (d) THF, CH₃COOH, H₂O, H₂, Pd(OH)₂/C; (e) (1) DCM, 5-phenyl-1*H*-tetrazole, (OBn)₂PN(*i*Pr)₂, 16 h (2) *m*CPBA, −78 °C-RT; (f) DBU, BSTFA; (g) MeOH, TFA; (h) (1) CDCl₃, 5-phenyl-1*H*-tetrazole, (OBn)₂PN(*i*Pr)₂, 3 h (2) *m*CPBA, −78 °C-RT; (i) MeOH, THF, 1 M TEAB, H₂, Pd(OH)₂/C, 72 h.

and is deemed highly challenging,⁵ particularly in view of their variable modes of action, different regioisomers and the limited chemical, and especially analytical, tools available. However, 5-PP-InsP₅ has been identified recently as the elusive regulator of Na⁺/K⁺-ATPase.⁶ The antifungal and anti-angiogenic drug itraconazole requires 5-PP-InsP₅ to inhibit cell motility.⁷ Additionally, the participation of the 5-PP-InsP₅ regioisomer, rather than InsP₆ or other inositol pyrophosphates [1-PP-InsP₅ and 1,5-(PP)₂-InsP₄] in glucose homeostasis was demonstrated.⁸ 5-PP-InsP₅ is thus a G-protein coupled receptor (GPCR) second messenger that is able to regulate synaptotagmin-7 (Sy7) dependent insulin release.⁹

As a result of such emerging important functions as above, expedient synthetic routes to generate inositol pyrophosphates and analogues,¹⁰ as well as tools to monitor their levels that could lead to the development of high throughput *in vitro* screening methods, are becoming more urgent and relevant. The ability to track the intracellular activity of 5-PP-InsP₅ quantitatively would be extremely useful for developing an accurate understanding of its cellular function. Moreover, library screening assay methodology might allow identification of druglike compounds to interfere with the enzymes of inositol pyrophosphate metabolism.

Molecular receptors that elicit a luminescence response upon binding a specific guest can provide a rapid and sensitive method for quantifying target species in aqueous biological media and living cells.^{11–14} Several molecular receptors for inositol phosphates in general have been developed for *in vitro* analyses;^{15–20} however, to the best of our knowledge there are no

examples of receptors selective for inositol pyrophosphates. Ansyn developed a receptor for inositol trisphosphates (InsP₃s) based on organic scaffolds substituted with phosphate-recognition moieties such as guanidinium or imidazolium groups.²¹ More recently, Bowman-James developed a supramolecular receptor for InsP₆, trapping the anion in host-guest sandwich structures involving two picolinamide macrocycles that bind InsP₆ *via* hydrogen bonding and electrostatic interactions.²²

To devise a molecular probe capable of the selective and sensitive detection of 5-PP-InsP₅ we first set out to develop an expedient new synthetic strategy of the ligand. The scalable synthesis and purification of such highly phosphorylated water-soluble ligands is generally deemed to be difficult, particularly in terms of protecting group strategies. Although routes to 5-PP-InsP₅ have been published, these often constructed the pyrophosphate group using a P(*v*) reagent to attach the β-phosphate precursor, in the process generating a highly unstable tri-protected P(*v*)-P(*v*) moiety before the final deprotection step.^{23,24} We chose to employ P(*iii*) methodology to build the pyrophosphate, resulting in the formation of a mixed P(*iii*)-P(*v*) anhydride prior to oxidation to form a di-protected P(*v*)-P(*v*) moiety. The use of such P(*iii*) phosphitylating agents has been adopted in the syntheses of other regioisomers of InsP₇ and InsP₈,^{25,26} as well as in our own work.^{27,28} A notable feature of the route in the present study is the use of the hydrogenation-resistant methylsulfonyl ethyl (MSE) groups to protect the phosphate attached to the 5-position.



Results and discussion

Synthesis of 5-PP-InsP₅

The route (Scheme 1, see also ESI) begins from 1,6:3,4-bis-[O-(2,3-dimethoxybutane-2,3-diyl)]-*myo*-inositol (**2**) synthesised from inositol, as described.²⁹ This was benzylated regioselectively at the axial 2-position hydroxyl, before being phosphorylated at the remaining exposed hydroxyl in the 5-position. The regioselectivity of this benzylation reaction has been observed before, although the reason for its occurrence is unknown.²⁹

This first phosphorylation employed a phosphoramidite to attach a phosphate precursor protected by methylsulfonylethyl (MSE) protecting groups to the 5-position. The bis[(methylsulfonyl) ethyl]diisopropylphosphoramidite (**4**) required was synthesised in 49% yield using a version of the method described.³⁰ Following oxidation with *m*CPBA, the protected monophosphate product (**5**) was collected in 93% yield. The BDA-protecting groups were removed with TFA to generate tetraol (**6**) in 88% yield. The benzyl group attached to the 2-position was cleaved *via* hydrogenation, and the product was lyophilised to generate pentaol (**7**) in 80% yield. The use of MSE-protecting groups was crucial during this step as they are resistant to hydrogenation, thereby enabling the easy selective removal of only the benzyl group attached to the 2-position. Phosphorylation using dibenzyl phosphoramidite then allowed benzyl-protected phosphate groups to be attached to the 1, 2, 3, 4 and 6-positions of the inositol ring. An excess of phosphoramidite and 5-phenyl-1*H*-tetrazole activator was required, but the phosphorylation was completed to generate the protected hexakisphosphate (**8**) in 97% yield. Use of a protecting group such as benzyl for the phosphates attached to these positions was necessary as it is an orthogonally-stable protecting group to the MSE groups attached to the phosphate at the 5-position. This enabled selective deprotection of the 5-position phosphate in the subsequent step to begin the construction of the pyrophosphate moiety only at this position.

The next stage was a multi-step sequence to construct the pyrophosphate moiety. These steps had to be performed in quick

succession as some of the intermediates proved to be unstable. The first step was the simultaneous cleavage of the base-labile MSE groups and silylation of the newly exposed phosphate with DBU and BSTFA. The next was removal of the silyl groups with methanol and TFA, the progress of which was confirmed using ³¹P NMR spectroscopy. After methanolysis, the product was dried thoroughly on a vacuum line. Phosphorylation of the deprotected 5-position phosphate was achieved using benzyl-protected phosphoramidite and 5-phenyl-1*H*-tetrazole to generate the mixed P(III)–P(V) anhydride that was subsequently oxidised using *m*CPBA to form the protected pyrophosphate (**9**). Importantly, an excess of 5-phenyl-1*H*-tetrazole was required during this phosphorylation to suppress competing cyclisation reactions. Following oxidation, the traditional aqueous work-up for phosphorylations was not carried out due to the instability of the protected pyrophosphate **9**, although **9** was sufficiently stable to survive purification *via* flash chromatography with a silica column that had been deactivated with triethylamine immediately before the final deprotection step. The benzyl groups of the protected pyrophosphate precursor were removed in a final hydrogenation step using Pearlman's catalyst and in the presence of TEAB buffer to provide a source of counterions. Addition of chelating agent EDTA was needed to obtain sharp signals in the initial ³¹P NMR spectrum of the crude product. The product 5-PP-InsP₅ was then purified through reverse-phase ion pair chromatography (0–10% MeCN in 0.05 M TEAB), with the phosphate-containing product fractions identified using a Briggs phosphate assay. The purified triethylammonium salt of 5-PP-InsP₅ (**1**, 35% isolated yield for the entire pyrophosphate formation sequence from compound **8**) was lyophilised to a colourless glass and was stored at –20 °C. It was more stable than initially expected, showing no signs of degradation by either ¹H NMR or ³¹P NMR spectroscopy when left at room temperature for over a month.

Molecular probe for 5-PP-InsP₅

A molecular probe of utility should be tuned to a physiological concentration range (0.5–5.0 μM) and display minimal interference from other inositol phosphates, particularly InsP₆. Luminescent lanthanide probes are attractive for this purpose as they

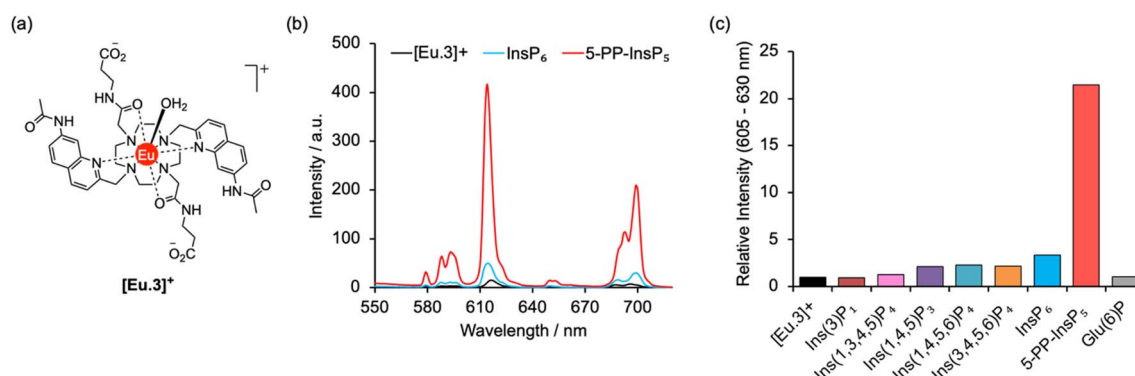


Fig. 2 Selective increase in emission of [Eu.3]⁺ for 5-PP-InsP₅. (a) Molecular structure of [Eu.3]⁺ (b) change in europium emission spectra of [Eu.3]⁺ (5 μM) in the presence of 250 μM 5-PP-InsP₅ (red line) and InsP₆ (blue line). (c) Large enhancement in intensity of the $\Delta J = 2$ emission band (605–630 nm) of [Eu.3]⁺ (5 μM) upon addition of 5-PP-InsP₅ compared with the negligible response with a range of inositol phosphates and glucose-6-phosphate (250 μM each). Measured in 10 mM HEPES, pH 7.0, 295 K, $\lambda_{\text{ex}} = 330$ nm.



offer long-lived emission enabling time-resolved measurements to remove background fluorescence from the sample, and line-like emission spectra that encode information about the local coordination environment.^{31–35} We previously developed a family of macrocyclic Eu(III) complexes whose luminescence is enhanced upon binding the nucleoside di- and triphosphates ADP and ATP, whereas all monophosphates caused much smaller changes in emission.^{36–39} Within this family we found that **[Eu.3]⁺** (Fig. 2a), bearing two quinoline arms and two neutral carbonyl amide donors, exhibits the strongest binding to ADP ($\log K_a = 5.7$)^{36,39} in aqueous solution and was therefore considered the lead candidate for sensing of 5-PP-InsP₅. The UV-Vis absorption spectrum of **[Eu.3]⁺** in aqueous buffer (10 mM HEPES, pH 7.0, 295 K) comprises a broad band centred at 330 nm (Fig. S1†). Upon excitation at 330 nm the complex displays emission in the red region of the visible spectrum, well separated from the absorption band and featuring a pronounced $\Delta J = 2$ band between 605–630 nm and two discernible components within the $\Delta J = 4$ band around 675–705 nm (Fig. S1†).

The ability of complex **[Eu.3]⁺** to bind and sense 5-PP-InsP₅ was examined in 10 mM HEPES buffer at pH 7.0. Addition of 250 μ M 5-PP-InsP₅ (50 equivalents) resulted in a substantial 22-fold enhancement in emission intensity of **[Eu.3]⁺** within the $\Delta J = 2$ band (605–630 nm) and subtle changes in spectral shape (Fig. 2b and S2†). This is consistent with coordination of the pyrophosphate group of 5-PP-InsP₅ to the Eu(III) metal centre and displacement of the bound water molecule, thereby reducing a major pathway for non-radiative decay of the Ln(III) ion's electronically excited state. In contrast, adding 250 μ M InsP₆ caused only a minor 3-fold increase in emission intensity, indicating a weak interaction with this anion. Similarly, very small changes in emission were observed for a wide range of common cellular inositols bearing phosphate groups to a variable degree and the carbohydrate glucose-6-phosphate (Fig. 2c and S3†).

Emission lifetimes of **[Eu.3]⁺** measured in H₂O and D₂O (Table 1) in the absence and presence of 5-PP-InsP₅ revealed a reduction in the number of bound water molecules, q , from one to zero (within experimental error), supporting direct coordination of 5-PP-InsP₅ to the Eu(III) centre. In comparison, we found that InsP₆ did not reduce the hydration state, consistent with very weak binding.

An apparent binding constant between **[Eu.3]⁺** and 5-PP-InsP₅ was determined by plotting the change in the intensity

Table 1 Emission lifetimes, hydration state q , and apparent binding constants for **[Eu.3]⁺** with 5-PP-InsP₅ and InsP₆ (measured in 10 mM HEPES at pH 7.0)

Sample	$\tau_{\text{H}_2\text{O}}^a/\text{ms}$	$\tau_{\text{D}_2\text{O}}^a/\text{ms}$	q^b	$\log K_a^c$
[Eu.3]⁺	0.560	1.223	0.86	n/a
InsP ₆	0.585	1.361	0.87	n.d.
5-PP-InsP ₅	1.000	1.205	−0.09	5.37 ± 0.50

^a Mean \pm standard deviation for two independent measurements.

^b Values of hydration state q (calculation error $\pm 20\%$) were derived using modified Horrocks equation.⁴⁰ ^c Mean \pm standard deviation for two independent measurements. n.d. = not determined due to minor changes in emission that prevented reliable data fitting.

ratio of the $\Delta J = 2/\Delta J = 1$ emission bands (605–630/580–600 nm) as a function of guest concentration, followed by curve fitting based on a 1 : 1 binding model (Fig. S4†). We measured a $\log K_a$ of 5.37 ± 0.50 , which is notably higher than that previously determined for the inorganic anion pyrophosphate ($\log K_a = 4.7$) under the same conditions, and slightly lower than for ADP ($\log K_a = 5.7$).³⁶ The small changes in emission intensity of **[Eu.3]⁺** towards InsP₆ prevented the accurate measurement of a binding constant. The possibility of a 2 : 1 **[Eu.3]⁺**:5-PP-InsP₅ complex was also considered, wherein 5-PP-InsP₅ is sandwiched between two Eu(III) complexes in a manner similar to that observed for InsP₆ by Bowman-James.²² However, fitting of the titration data of **[Eu.3]⁺** with 5-PP-InsP₅ to a 2 : 1 binding model showed no improvement in fitting compared with the 1 : 1 binding model (difference in the covariance of fit = 2.0 and substantial errors in the binding constants were observed).§

As a consequence of the higher affinity of **[Eu.3]⁺** for 5-PP-InsP₅ over pyrophosphate, an approximate 2-fold greater increase in emission intensity was found with the former anion, enabling these two substrates to be readily distinguished (Fig. S5†). Moreover, it was possible to discriminate between 5-PP-InsP₅ and the nucleoside diphosphate ADP by their unique emission spectral shapes originating from differences in coordination environment at the metal centre, despite their similar overall binding affinities and overall increases in emission.

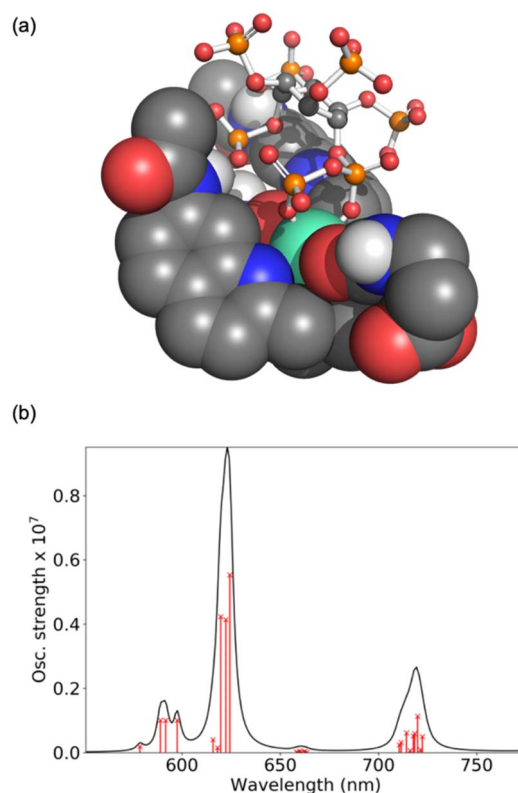


Fig. 3 Computational analysis of 5-PP-InsP₅ binding to **[Eu.3]⁺**: (a) DFT optimised geometry of the bidentate binding mode and (b) *ab initio* luminescence spectrum from ⁵D₀ showing the individual microstates of the ⁷F term as red crosses on lines proportional to their oscillator strength.



Specifically, 5-PP-InsP₅ gives rise to a single intense peak within the $\Delta J = 2$ band at 615 nm (Fig. S5†), whereas ADP induces a prominent shoulder peak at 623 nm alongside a larger band at 617 nm. Further, within the $\Delta J = 4$ band, 5-PP-InsP₅ causes a pronounced peak at 700 nm, whereas ADP produces two equally intense bands in this region at 690 nm and 703 nm.

Thus, we have identified a luminescent probe that can bind and sense 5-PP-InsP₅ with minimal interference from a variety of molecules bearing multiple phosphate and pyrophosphate groups. It should be noted that the regioisomer 1-PP-InsP₅ (Fig. S6†) produces a similar, albeit less pronounced, emission change to 5-PP-InsP₅. However, to the best of our knowledge no biological role has yet been identified for 1-PP-InsP₅ (or indeed its enantiomer 3-PP-InsP₅) that would merit the development of a sensor for its selective detection. Additionally, ATP induces an emission enhancement³⁶ that would likely interfere with the recognition of 5-PP-InsP₅ in more complex biological environments. Importantly, we do not anticipate such interference being an issue when applying the probe to *in vitro* enzyme monitoring or high throughput screening.

Computational analysis of host-guest binding structures and luminescence spectra

Computations were performed to obtain further insight into host-guest binding involved in the luminescence sensing of 5-PP-InsP₅. Structure optimizations using density functional theory

(DFT)^{41–43} revealed that the most stable binding mode for 5-PP-InsP₅ corresponds to bidentate binding of the pyrophosphate group (see Fig. 3a). One of the quinoline arms is rotated away from the Eu(III) centre to open the second binding site needed for bidentate binding, as illustrated in Fig. S11.† The bidentate binding mode was lower in free energy by 9.2 kJ mol⁻¹ compared to the second most stable binding mode featuring monodentate binding *via* the axial phosphate group, as shown in Fig. S12.† This change in free energy by 9.2 kJ mol⁻¹ corresponds to a decreased binding constant by about a factor 40. This means that about 1 out of 40 bound 5-PP-InsP₅ molecules would occupy the monodentate mode, whereas the remaining are bound in a bidentate fashion. Binding of InsP₆ in a monodentate manner (Fig. S13†) was found to be significantly weaker than either the monodentate or the bidentate binding mode of 5-PP-InsP₅.

To understand the enhanced binding of 5-PP-InsP₅ relative to pyrophosphate, we have analysed the presence of hydrogen bonds within the complex. Indeed, as shown in Fig. S11,† we find three hydrogen bonds between 5-PP-InsP₅ and the macrocyclic ligand. Two of these involve the axial phosphate (2P) group binding to amide hydrogens of [Eu.3]⁺ and the third involves an equatorial phosphate (3P) group binding to the dissociated quinoline amide arm.

The simulated luminescence spectrum⁴⁴ for PP-InsP₅ is shown in Fig. 3b, including transitions from the ⁵D₀ state to the 49 microstates of the ⁷F term. The individual microstates are

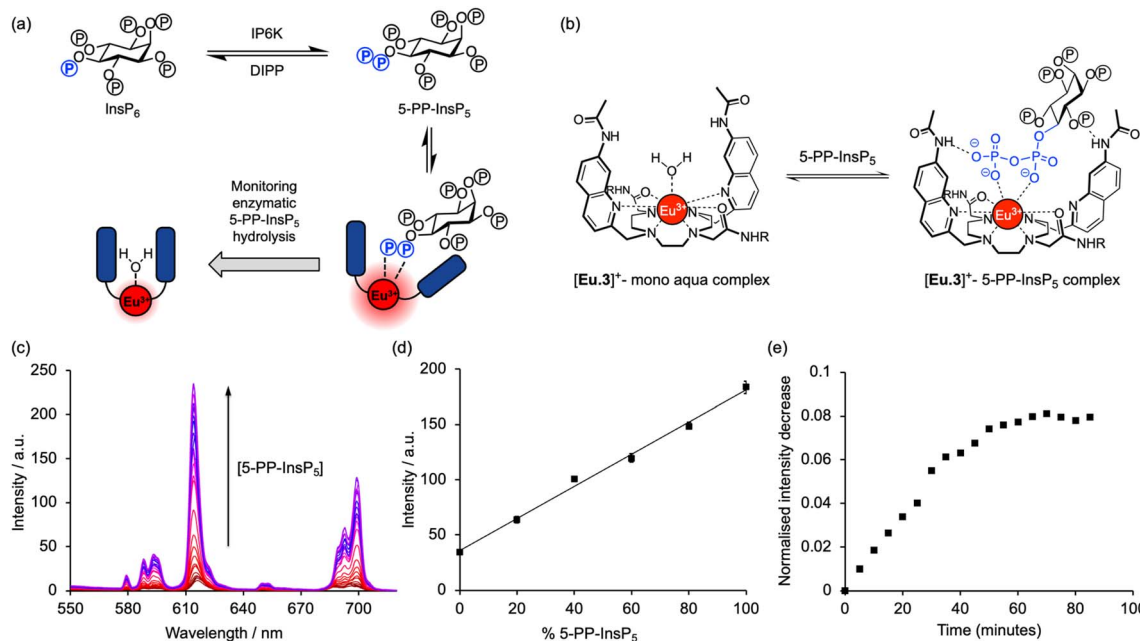


Fig. 4 [Eu.3]⁺ can be used to monitor enzymatic hydrolysis of 5-PP-InsP₅ to InsP₆ by NUDT3. (a) Principle of luminescence monitoring of the reversible interconversion between PP-InsP₅/InsP₆ catalysed by IP6K/DIPP enzymes. [Eu.3]⁺ selectively binds 5-PP-InsP₅ reporting its production or consumption by an increase or decrease in emission during the course of the reaction. (b) Schematic depiction of the proposed binding mode of [Eu.3]⁺ to the pyrophosphate moiety of 5-PP-InsP₅. (c) Enhancement in Eu(III) emission spectra upon incremental addition of 5-PP-InsP₅ (up to 1 mM). (d) Enzyme simulation reaction demonstrating a linear increase in time-resolved emission with increasing molar ratio of 5-PP-InsP₅/InsP₆. Data are mean \pm SEM ($r^2 > 0.99$) from experiments performed using 5 μ M [Eu.3]⁺, 100 μ M total 5-PP-InsP₅ + InsP₆ in 10 mM HEPES, pH 7.0. (e) Representative real-time NUDT3 enzyme reaction conducted in triplicate and corrected for emission decay using identical assay mixture but omitting enzyme. Conditions: 5 μ M [Eu.3]⁺, 100 μ M 5-PP-InsP₅, 1.6 μ g NUDT3, 50 mM KCl, 0.05 mg mL⁻¹ BSA in 40 μ L of 10 mM HEPES, pH 7.0, 295 K. For all experiments: $\lambda_{\text{ex}} = 292\text{--}366$ nm, $\lambda_{\text{em}} = 615\text{--}625$ nm, integration time = 60–400 μ s.



shown as red lines while the overall convoluted spectrum is shown in black. The simulated spectrum features a $\Delta J = 1$ band split into two peaks followed by a single $\Delta J = 2$ peak dominating the spectrum, and finally a $\Delta J = 4$ band comprising one major peak. It agrees well with the experimental spectrum (Fig. 2b) in all these aspects, further supporting the validity of the computational model.⁴⁵ Further spectra are shown in the ESI† highlighting the increase in the $\Delta J = 2$ band with PP-InsP₅ (and InsP₆) compared with the water-bound complex (Fig. S9†).

Monitoring enzymatic reactions involving 5-PP-InsP₅

The high binding affinity of 5-PP-InsP₅ to [Eu.3]⁺ combined with the striking increase in emission intensity and lifetime, compared with the much more subtle emission changes seen with InsP₆ (and other inositol and carbohydrate phosphates), enabled a new luminescence method to discriminate 5-PP-InsP₅ from InsP₆ effectively. We exploited this to develop a microplate assay for real-time monitoring of the activity of pyrophosphatase NUDT3 (UniProt: O95989), a DIPP phosphatase enzyme that hydrolyses the pyrophosphate group of 5-PP-InsP₅ to generate InsP₆ (Fig. 4a).

Initially, we confirmed the stability of the emission response of [Eu.3]⁺ with 5-PP-InsP₅ over a 60 minutes incubation period (Fig. S6†). Next, we simulated the conversion of 5-PP-InsP₅ into InsP₆ (or *vice versa*) by changing the molar ratio of InsP₆/5-PP-InsP₅ systematically. The linear increase in time-resolved emission intensity of [Eu.3]⁺ with increasing mole fraction of 5-PP-InsP₅ is shown in Fig. 4d. A similar linear relationship was found in the presence of bovine serum albumin, a common additive in enzyme assays (Fig. S7†). These data suggested that the luminescence signal of [Eu.3]⁺ could be correlated with the progress of a pyrophosphatase reaction.

To confirm this, we incubated the enzyme, NUDT3 with 5-PP-InsP₅ in 10 mM HEPES buffer (containing 100 μ M 5-PP-InsP₅, 50 mM KCl, 0.05 mg mL⁻¹ BSA)⁴⁶ and were able to observe a progressive decrease in time-resolved emission intensity over 90 minutes (Fig. 4e) as NUDT3 hydrolyses 5-PP-InsP₅ to InsP₆. We have utilised the long-lived emission of [Eu.3]⁺ to record time-resolved emission measurements (615–625 nm, integration time = 60–400 μ s), thereby removing any short-lived fluorescence arising from components in the assay sample, thus increasing signal to noise ratio.

Conclusion

We have discovered that a coordinately unsaturated cationic lanthanide complex can be used to detect selectively the inositol pyrophosphate cellular second messenger 5-PP-InsP₅ with low micromolar sensitivity and without interference from InsP₆ and other common cellular inositol and carbohydrate phosphates. 5-PP-InsP₅ was prepared *via* a new synthetic approach. The combination of selective binding of [Eu.3]⁺ to 5-PP-InsP₅ and the resulting emission enhancement was exploited to develop a real-time assay for monitoring the enzymatic conversion 5-PP-InsP₅ to InsP₆. Our enzymatic assay was conducted in time-resolved format to exploit the long luminescence lifetime of [Eu.3]⁺, and thus improve signal-to-noise ratio, and in multi-well plates

importantly demonstrating its potential suitability for high-throughput use. The assay is label-free and does not require expensive antibodies or chemical modification of the substrate with a fluorescent or radioactive label. Its availability should have a significant impact on the study of protein dephosphorylation and emerging cellular signalling pathways regulated by 5-PP-InsP₅, not least those involved in glucose homeostasis.

Data availability

ESI is available, including synthetic procedures, compound characterisation, and photophysical studies of host-guest interactions.†

Author contributions

M. L. S.: synthesis and characterisation of compounds. F. A. J. and S. W.: europium probe studies, anion binding and sensing experiments, enzyme assay development. F. P.: computation, supervision of modelling studies, data analysis. A. M. R.: supervision and development of synthetic methods, data analysis. B. V. L. P.: conceptualisation, funding acquisition, supervision of synthetic aspects, data analysis, writing and editing of the manuscript. S. J. B.: conceptualisation, funding acquisition, supervision of europium probe studies, methodology, data analysis, writing and editing of the manuscript. All authors have contributed to, seen and approved the manuscript.

Conflicts of interest

There are no conflicts to declare.

Acknowledgements

This work was funded by a Biotechnology and Biotechnological Sciences Research Council Tools and Resources Development Grant [BB/T012099/1] to SJB. BVL is a Wellcome Trust Senior Investigator (Grant 101010). We thank Erin Robertson (Loughborough University) for initial screening of Eu(III) probes for binding to 5-PP-InsP₅. This research was funded by the Wellcome Trust. For the purpose of Open Access, the authors have applied a CC BY public copyright licence to any Author Accepted Manuscript version arising from this submission.

Notes and references

§ The luminescence titration data of [Eu.3]⁺ with 5-PP-InsP₅ was fitted to both a 1 : 1 and 2 : 1 binding model using Bindfit [<https://www.supramolecular.org>]. The covariance of fit (cov_{fit}) allowed comparison of the quality of the curve fitting between the 1 : 1 and 2 : 1 binding models (see ESI Fig. S4†). Due to the higher number of parameters from the 2 : 1 binding model, an improvement in the cov_{fit} by a factor greater than 3 should indicate that the 2 : 1 binding model is preferential.⁴⁷ However, compared with the 1 : 1 binding model [Eu.3]⁺ showed no improvement in fitting for the 2 : 1 binding model, with $F \text{cov}_{\text{fit}} = 2.0$ and much larger errors in the estimated binding constants.

- 1 S. B. Shears, *J. Cell. Physiol.*, 2018, **233**, 1897–1912.
- 2 S. B. Shears, *Adv. Biol. Regul.*, 2015, **57**, 203–216.



- 3 A. Chakraborty, *Biol. Rev.*, 2018, **93**, 1203–1227.
- 4 M. P. Thomas and B. V. L. Potter, *FEBS J.*, 2014, **281**, 14–33.
- 5 M. Nguyen Trung, D. Furkert and D. Fiedler, *Curr. Opin. Chem. Biol.*, 2022, **70**, 102177.
- 6 A. C. Chin, Z. Gao, A. M. Riley, D. Furkert, C. Wittwer, A. Dutta, T. Rojas, E. R. Semenza, R. A. Felder, J. L. Pluznick, H. J. Jessen, D. Fiedler, B. V. L. Potter, S. H. Snyder and C. Fu, *Sci. Adv.*, 2020, **6**, eabb8542.
- 7 J. Qi, W. Cheng, Z. Gao, Y. Chen, M. L. Shipton, D. Furkert, A. C. Chin, A. M. Riley, D. Fiedler, B. V. L. Potter and C. Fu, *Biomed. Pharmacother.*, 2023, **161**, 114449.
- 8 X. Zhang, N. Li, J. Zhang, Y. Zhang, X. Yang, Y. Luo, B. Zhang, Z. Xu, Z. Zhu, X. Yang, Y. Yan, B. Lin, S. Wang, D. Chen, C. Ye, Y. Ding, M. Lou, Q. Wu, Z. Hou, K. Zhang, Z. Liang, A. Wei, B. Wang, C. Wang, N. Jiang, W. Zhang, G. Xiao, C. Ma, Y. Ren, X. Qi, W. Han, C. Wang and F. Rao, *Nat. Metab.*, 2021, **3**, 1400–1414.
- 9 B. Tu-Sekine and S. F. Kim, *Int. J. Mol. Sci.*, 2022, **23**, 6747.
- 10 S. B. Shears and H. Wang, *Molecules*, 2020, **25**, 4515.
- 11 D. A. McNaughton, M. Fares, G. Picci, P. A. Gale and C. Caltagirone, *Coord. Chem. Rev.*, 2021, **427**, 213573.
- 12 L. You, D. Zha and E. V. Anslyn, *Chem. Rev.*, 2015, **115**, 7840–7892.
- 13 A. B. Aletti, D. M. Gillen and T. Gunnlaugsson, *Coord. Chem. Rev.*, 2018, **354**, 98–120.
- 14 T. D. Ashton, K. A. Jolliffe and F. M. Pfeffer, *Chem. Soc. Rev.*, 2015, **44**, 4547–4595.
- 15 S. Kaur, S. Pramanik, V. W. Day and K. Bowman-James, *Dalton Trans.*, 2021, **50**, 480–484.
- 16 M. Reinmuth, S. Pramanik, J. T. Douglas, V. W. Day and K. Bowman-James, *Eur. J. Inorg. Chem.*, 2019, **2019**, 1870–1874.
- 17 K. Reeh, P. A. Summers, I. R. Gould, R. Woscholski and R. Vilar, *Sci. Rep.*, 2020, **10**, 18450.
- 18 D. Quinone, N. Veiga, J. Torres, J. Castiglioni, C. Bazzicalupi, A. Bianchi and C. Kremer, *Dalton Trans.*, 2016, **45**, 12156–12166.
- 19 N. Veiga, J. Torres, C. Bazzicalupi, A. Bianchi and C. Kremer, *Chem. Commun.*, 2014, **50**, 14971–14974.
- 20 S. M. Butterfield, D.-H. Tran, H. Zhang, G. D. Prestwich and S. Matile, *J. Am. Chem. Soc.*, 2008, **130**, 3270–3271.
- 21 E. V. Anslyn and J. B. Shear, *Chem. Biol.*, 2002, **9**, 779–780.
- 22 S. Pramanik, V. W. Day and K. Bowman-James, *Chem. Commun.*, 2020, **56**, 3269–3272.
- 23 M. Wu, B. E. Dul, A. J. Trevisan and D. Fiedler, *Chem. Sci.*, 2013, **4**, 405–410.
- 24 H. J. Jessen, S. Capolicchio, I. Pavlovic and D. T. Thakor, *Synlett*, 2014, **25**, 1494–1498.
- 25 S. Capolicchio, D. T. Thakor, A. Linden and H. J. Jessen, *Angew. Chem., Int. Ed.*, 2013, **52**, 6912–6916.
- 26 S. Capolicchio, H. Wang, D. T. Thakor, S. B. Shears and H. J. Jessen, *Angew. Chem., Int. Ed.*, 2014, **53**, 9508–9511.
- 27 H. Wang, H. Y. Godage, A. M. Riley, J. D. Weaver, S. B. Shears and B. V. L. Potter, *Chem. Biol.*, 2014, **21**, 689–699.
- 28 A. M. Riley, J. E. Unterlass, V. Konieczny, C. W. Taylor, T. Helleday and B. V. L. Potter, *MedChemComm*, 2018, **9**, 1105–1113.
- 29 A. M. Riley, H. Wang, J. D. Weaver, S. B. Shears and B. V. L. Potter, *Chem. Commun.*, 2012, **48**, 11292–11294.
- 30 S. B. Engelsma, N. J. Meeuwenoord, H. S. Overkleeft, G. A. van der Marel and D. V. Filippov, *Angew. Chem., Int. Ed.*, 2017, **56**, 2955–2959.
- 31 J.-C. G. Bünzli, *Coord. Chem. Rev.*, 2015, **293–294**, 19–47.
- 32 E. G. Moore, A. P. S. Samuel and K. N. Raymond, *Acc. Chem. Res.*, 2009, **42**, 542–552.
- 33 D. Parker, J. D. Fradgley and K.-L. Wong, *Chem. Soc. Rev.*, 2021, **50**, 8193–8213.
- 34 S. E. Bodman and S. J. Butler, *Chem. Sci.*, 2021, **12**, 2716–2734.
- 35 S. E. Bodman, C. Breen, S. Kirkland, S. Wheeler, E. Robertson, F. Plasser and S. J. Butler, *Chem. Sci.*, 2022, **13**, 3386–3394.
- 36 R. Mailhot, T. Traviss-Pollard, R. Pal and S. J. Butler, *Chem. – Eur. J.*, 2018, **24**, 10745–10755.
- 37 S. H. Hewitt, J. Parris, R. Mailhot and S. J. Butler, *Chem. Commun.*, 2017, **53**, 12626–12629.
- 38 S. H. Hewitt, R. Ali, R. Mailhot, C. R. Antonen, C. A. Dodson and S. J. Butler, *Chem. Sci.*, 2019, **10**, 5373–5381.
- 39 S. H. Hewitt, G. Macey, R. Mailhot, M. R. J. Elsegood, F. Duarte, A. M. Kenwright and S. J. Butler, *Chem. Sci.*, 2020, **11**, 3619–3628.
- 40 A. Beeby, I. M. Clarkson, R. S. Dickins, S. Faulkner, D. Parker, L. Royle, A. S. de Sousa, J. A. Gareth Williams and M. Woods, *J. Chem. Soc., Perkin Trans. 2*, 1999, 493–504.
- 41 N. Mardirossian and M. Head-Gordon, *J. Chem. Phys.*, 2016, **144**, 214110.
- 42 E. Epifanovsky, A. T. Gilbert, X. Feng, J. Lee, Y. Mao, N. Mardirossian, P. Pokhilko, A. F. White, M. P. Coons, A. L. Dempwolff and et al., *J. Chem. Phys.*, 2021, **155**, 084801.
- 43 F. Neese, *Wiley Interdiscip. Rev.: Comput. Mol. Sci.*, 2022, **12**, e1606.
- 44 I. F. Galván, M. Vacher, A. Alavi, C. Angeli, F. Aquilante, J. Autschbach, J. J. Bao, S. I. Bokarev, N. A. Bogdanov, R. K. Carlson, L. F. Chibotaru, J. Creutzberg, N. Dattani, M. G. Delcey, S. S. Dong, A. Dreuw, L. Freitag, L. M. Frutos, L. Gagliardi, F. Gendron, A. Giussani, L. González, G. Grell, M. Guo, C. E. Hoyer, M. Johansson, S. Keller, S. Knecht, G. Kovačević, E. Källman, G. Li Manni, M. Lundberg, Y. Ma, S. Mai, J. P. Malhado, P. Å. Malmqvist, P. Marquetand, S. A. Mewes, J. Norell, M. Olivucci, M. Oppel, Q. M. Phung, K. Pierloot, F. Plasser, M. Reiher, A. M. Sand, I. Schapiro, P. Sharma, C. J. Stein, L. K. Sørensen, D. G. Truhlar, M. Ugandi, L. Ungur, A. Valentini, S. Vancoillie, V. Veryazov, O. Weser, T. A. Wesolowski, P.-O. Widmark, S. Wouters, A. Zech, J. P. Zobel and R. Lindh, *J. Chem. Theory Comput.*, 2019, **15**, 5925–5964.
- 45 S. E. Bodman, C. Breen, F. Plasser and S. J. Butler, *Org. Chem. Front.*, 2022, **9**, 5494–5504.
- 46 R. S. Kilari, J. D. Weaver, S. B. Shears and S. T. Safrany, *FEBS Lett.*, 2013, **587**, 3464–3470.
- 47 P. Thordarson, *Chem. Soc. Rev.*, 2011, **40**, 1305–1323.

